



ELSEVIER

Physica D 99 (1996) 359–368

PHYSICA D

Phase-field simulations and experiments of faceted growth in liquid crystals

R. González-Cinca^a, L. Ramírez-Piscina^a, J. Casademunt^b, A. Hernández-Machado^{b,*},
L. Kramer^c, T. Tóth Katona^d, T. Börzsönyi^d, Á. Buka^d

^a *Departament de Física Aplicada, Universitat Politècnica de Catalunya, Campus Nord-Ed. B5, J. Girona Salgado s/n, E-08034 Barcelona, Spain*

^b *Departament E.C.M., Fac. de Física, Universitat de Barcelona, Diagonal 647, E-08028 Barcelona, Spain*

^c *Institute of Physics, University of Bayreuth, E-95440 Bayreuth, Germany*

^d *KFKI, Research Institute for Solid State Physics, Hungarian Academy of Sciences, P.O.B. 49, H-1525 Budapest, Hungary*

Received 3 January 1996; accepted 13 May 1996

Communicated by H. Müller-Krumbhaar

Abstract

We present numerical simulations directed at the description of smectic-B germs growing into the supercooled nematic phase for two different liquid crystalline substances. The simulations are done by means of a phase-field model appropriate to study strong anisotropy and also faceted interfaces. The most important ingredient is the angle-dependent surface energy, but kinetic effects are also relevant. The simulations reproduce qualitatively a rich variety of morphologies observed in the experiments for different values of undercooling, extending from the faceted equilibrium shape to fully developed dendrites.

PACS: 61.30.-v; 61.50.Cj; 81.30.Fb; 68.70.+w

1. Introduction

Dendritic growth is one of the most interesting phenomena in pattern forming instabilities. It occurs in a rich variety of situations not only in the context of crystal growth, but also in other interfacial growth phenomena such as mesophase transitions in liquid crystals, electrodeposition and expanding bacterial colonies [1–6]. In our present understanding, anisotropy seems to be an essential ingredient of the mechanisms that lead to the formation of dendrites

and the determination of their shape and growth velocity under given conditions [7,8].

An aspect which has received much attention recently is the case of faceted dendrites. The experimental observation [9] triggered substantial theoretical work [10–13]. Also directional solidification of faceted interfaces has been investigated theoretically [14–17] and experimentally, both in mesophase growth [17–20] and actual solidification [21–23].

In this paper we will focus on the case of liquid crystals, and in particular on the growth of a smectic-B phase into a supercooled nematic phase. Whereas nematics are fully liquid (no translational order), the smectic-B phase is characterized by strongly ordered

* Corresponding author.

layers with hexagonal order within the layers¹. This situation has been extensively studied experimentally during the last years and presents a rich variety of morphologies, ranging from strongly anisotropic equilibrium shapes with long facets, to apparently the usual non-faceted type of dendrites [26,28]. This is therefore an appropriate system to study the interplay between equilibrium anisotropy and dynamic effects in the growth morphology.

We have considered two different liquid crystals. One of the substances has been previously studied experimentally in [27,28] showing the different morphologies referred to above. Some new experimental results are also reported here. Experiments are done in very thin samples, which give a quasi-two-dimensional geometry in which the interface can be described by a line. The sample is initially set above the phase transition temperature T_{ns} , and is suddenly undercooled below this temperature in such a way that small germs of smectic-B nucleate and start to grow.

The growth of liquid crystal interfaces is in many aspects analogous to that of solidification interfaces. The basic description is expected to be the same, the main differences are in the parameter ranges, which often make the liquid crystal case particularly suitable from an experimental point of view. From a theoretical point of view, a significant parameter difference with respect to the solidification case is the one associated to the diffusion coefficients which are of the same order of magnitude in the two liquid crystal phases.

The standard macroscopic solidification model relies on the heat diffusion equation for the temperature field supplemented with boundary conditions (heat conservation and the Gibbs–Thomson local equilibrium relation) at the interface, which is assumed to be sharp. In rapid growing conditions the Gibbs–Thomson equation should have a kinetic term added, which accounts for deviations from the local equilibrium. This defines a free boundary problem that can be recast into an integrodifferential equation, which was the starting point for considerable numerical and ana-

lytical work. However, in the last years the so-called phase-field models, in which boundary conditions at the interface are avoided by defining an auxiliary field that mimics an order parameter, have received increased attention. We will show that this procedure is also suitable and competitive in cases with faceted interfaces, corresponding to cusps in the surface tension function $\sigma(\theta)$.

This approach has been successfully applied to ordinary dendritic crystal growth [29–35], but neither to situations with strong anisotropy nor to cases in which the equilibrium interface presents facets in some preferred directions. In such cases, the interfacial free energy, which can be extracted from the equilibrium shape through the Wulff construction, has non-analiticities (cusps) in its angular dependence, associated to such preferred directions. The phase-field approach will also allow for an anisotropy of the kinetic effects, which can be chosen independently of the equilibrium anisotropy. The competition between the two anisotropies may also induce morphological changes as a function of undercooling [36]. For simplicity and as a first step, in this paper we will restrict ourselves mainly to the case of isotropic kinetic effects [10]. We will show that even with this choice the phase-field model can qualitatively reproduce the patterns observed in the experiments.

Experimental results for these substances are presented in Section 2. In Section 3 we describe the model, in Section 4 the simulation procedure is presented together with the corresponding numerical results. Finally, the conclusions are drawn in Section 5.

2. Experimental system

We have studied the growth of two liquid crystalline substances, both presenting a nematic to smectic-B first-order phase transition. The first substance, 4-n-propyl-4'-cyano-trans 1,1-bicyclohexane, which will be called substance I, has a transition temperature $T_{ns} = 56.3^\circ\text{C}$. Substance I has already been experimentally studied in [27,28]. For the second substance, 4-n-butyl-4'-cyano-trans 1,1-bicyclohexane, which will be called substance II, the transition temperature is $T_{ns} = 53.1^\circ\text{C}$. We have focused on the study of the

¹ We are dealing with what is now usually called the “crystal B” phase, which has a weak 3D ordering, rather than the less common “hexatic B” phase, see, e.g. [24,25].

morphologies obtained in very thin samples, when the smectic and nematic directors are oriented parallel to the glass plates on both sides of the interface, the *P*(in *P*) case. In this situation, substance II shows a more elongated equilibrium shape than substance I. The long, faceted sides of the germs are parallel with the smectic layers (perpendicular to the director). The anisotropy of the surface tension $\sigma(0)/\sigma_{\frac{1}{2}(\pi)}$ is equal to the length-to-width ratio of these equilibrium shapes and it was found to be ≈ 4.8 for substance I and ≈ 18 for substance II. ($\theta = 0$ corresponds to the direction normal to the middle of the shorter, rough side.) The full angular dependence can be obtained from the Wulff construction (see [27,28] and is described by the function $\eta(\theta) = \sigma(\theta)/\sigma(0)$. We here take²

$$\begin{aligned}\eta_I(\theta) &= 1.000 - 0.353\theta^2 + 0.008\theta^4, \\ \eta_{II}(\theta) &= 1.000 - 0.445\theta^2 + 0.026\theta^4\end{aligned}\quad (2.1)$$

in the range $|\theta| \leq \frac{1}{2}\pi$, while $\eta(\theta) = \eta(\pi - \theta)$. Clearly $\eta(\theta)$ has cusps at $\theta = \pm\frac{1}{2}\pi$.

When the sample is suddenly undercooled with a temperature ΔT below the transition temperature T_{ns} , some smectic-B germs appear and grow, giving rise to different growing shapes or morphologies. For substance I, four different morphologies have been described for different undercooling conditions [27]. For small undercooling the experiment shows a very slow growth of the germ, which in the observed times maintains a rectangle-like shape very similar to the equilibrium one with two parallel facets and two rough convex sides (Fig. 1(a), where $\Delta = c_p\Delta T/L$ is the dimensionless undercooling). For slightly larger undercooling, the short sides undergo a first instability from convex to concave (Fig. 1(b)). For larger values of undercooling the faceted sides start to bend adopting a slightly concave curvature and (macroscopic) facets disappear with the four corners opened up, forming a butterfly-like shape (Fig. 1(c)). It is remarkable that the direction of the propagation velocity of the four tips in this morphology defines an angle with the smectic director which is not singled out in the equilibrium

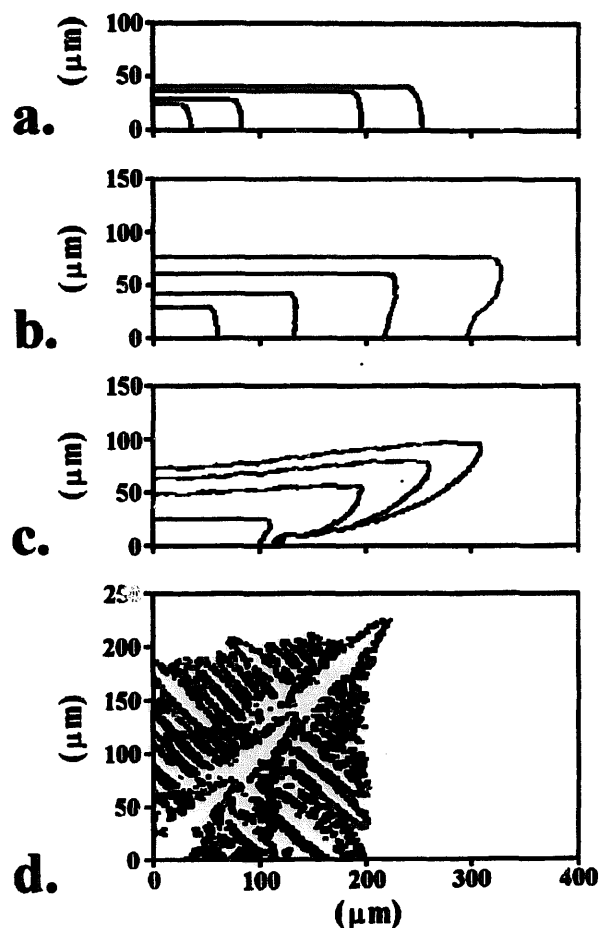


Fig. 1. Substance I. One quarter of the experimental microscopic images of the nematic–smectic-B interface demonstrated by plotting the contours of the patterns taken at subsequent times on top of each other: (a) $\Delta = 0.006$, $t = 11.7$ s; 1 min 23.7 s; 6 min 54.7 s; 10 min 8.1 s (b) $\Delta = 0.007$, $t = 32.8$ s; 1 min 53 s; 4 min 13.3 s; 7 min 58.4 s; (c) $\Delta = 0.009$, $t = 8.3$ s; 17.1 s; 23.4 s; 28.1 s; (d) $\Delta = 0.07$, $t = 0.2$ s; 0.4 s; 0.6 s.

anisotropy of the substance, and thus is presumably dynamically selected. For large undercooling the four main dendrites are obtained at angles close to 45° with the smectic layers (angle between the branches $\alpha \approx 90^\circ$), giving rise to an apparent fourfold symmetry which is absent in the equilibrium properties of the substance (Fig. 1(d)).

With regard to dynamics, in the quasi-equilibrium regime ($\Delta = 0.007$) growth velocities vary like $t^{-\gamma}$, with experimental values of γ in the range of 0.7 ± 0.2 , more or less compatible with diffusive slowing down ($\gamma = 0.5$). In the intermediate ($0.007 < \Delta < 0.015$) and fast ($\Delta > 0.015$) regimes, growth velocities tend to be asymptotically constant.

² Note that in [27] there are typographical errors in the formula for the quantity corresponding to $\eta_I(\theta)$ given in Fig. 2: a zero is missing in the last term and its sign is reversed.

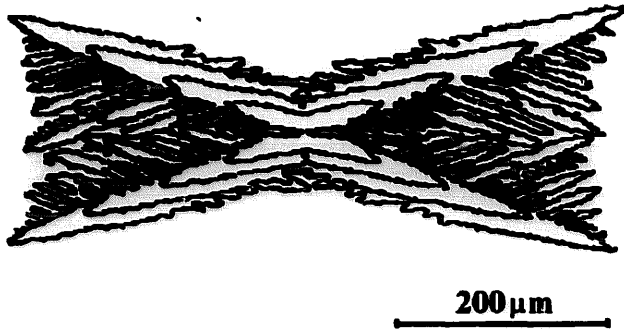


Fig. 2. Substance II. Experimental observation of the rapidly growing nematic–smectic-B interface, demonstrated in the same way as in Fig. 1. $\Delta = 0.086$, $t = 0.5$ s; 0.9 s; 1.3 s; 1.8 s.

As mentioned before, substance II shows a stronger anisotropy compared to that of substance I, with longer faceted sides compared to the rough ones in the equilibrium shapes. For small undercoolings a smectic-B germ of this material does not show non-equilibrium growth, e.g. it remains in a regime demonstrated in Fig. 1(a) and (b). In the large undercooling regime, this substance also displays a shape with four main dendrites arising from the corners of the equilibrium shape, but with smaller angles with the smectic layers. In contrast to substance I the angle $\frac{1}{2}\alpha$ showed a large variability ranging from 7° to 32° depending on the nucleation point (Fig. 2). Like for substance I, such angles do not appear as preferred in the equilibrium shape and presumably have a dynamical origin. Also, for substance II, the angle between the orientation of the germ, fixed by the smectic director, and the director of the surrounding nematic, showed considerable variability, again in contrast to substance I, where the angle between the two directors was always smaller than about 3° . A more detailed experimental study of these variabilities will be published elsewhere [37].

3. Phase-field model

The standard (sharp interface) model for free solidification of an anisotropic substance is defined by the heat diffusion equation and the boundary conditions at the interface:

$$\frac{\partial T}{\partial t} = D\nabla^2 T, \quad (3.1)$$

$$L\nu_n = Dc_p[(\nabla_n T)_{\text{smectic-B}} - (\nabla_n T)_{\text{nematic}}], \quad (3.2)$$

$$T_{\text{interface}} = T_{\text{ns}} - \frac{T_{\text{ns}}}{L}[\sigma(\theta) + \sigma''(\theta)]\kappa - \frac{\nu_n}{\mu(\theta)}, \quad (3.3)$$

where D is the thermal diffusion constant which we assume to be the same in both phases (symmetric model), L is the latent heat per unit volume, c_p is the specific heat per unit volume, ∇_n is the normal derivative at the interface, ν_n is the normal velocity and κ is the local curvature of the interface, $\mu(\theta)$ is an anisotropic kinetic coefficient and θ is the angle between the normal to the nematic–smectic-B interface and the x -axis chosen parallel to the smectic layers. The surface free energy $\sigma(\theta)$ also depends on the local interface orientation. Primes denote derivatives with respect to θ .

Clearly, the (generalized) Gibbs–Thomson relation (3.3) can pose a problem in the faceted case, since $\sigma''(\theta)$ then becomes singular. Regularization procedures have been presented and analysed for freely growing needle crystals in the case of weak faceting [10–12]. The subtleties encountered there in the limit of low surface tension on the rough parts are presumably not relevant in our context. Also, some simulations with faceted needle crystals have been performed [13].

In our simulations we have employed a phase-field model where the heat diffusion equation couples through a source term to an equation for an order parameter, which changes continuously across the interface. By the nature of such models, a new parameter appears, the interfacial thickness, that controls the convergence to the sharp interface limit. In the integration of the equations there is no distinction between bulk and interface. Also, the (relaxative) dynamics of the order parameter naturally leads to kinetic effects, analogous to that in the last term of Eq. (3.3), whose magnitude can be controlled by the relaxation time. Anisotropy in the (equilibrium) surface free energy and in the kinetic term can be straightforwardly implemented in the formulation proposed by Wheeler et al. [30–33], which is thermodynamically consistent and converges to Eqs. (3.1)–(3.3) in the sharp interface limit [31,38]. This model is defined by the following equations, which we present directly in dimensionless

form:

$$\begin{aligned} \epsilon^2 \tau(\theta) \frac{\partial \phi}{\partial t} = & \phi(1 - \phi) \left(\phi - \frac{1}{2} + 30\epsilon\beta\Delta u\phi(1 - \phi) \right) \\ & - \epsilon^2 \frac{\partial}{\partial x} \left(\eta(\theta)\eta'(\theta) \frac{\partial \phi}{\partial y} \right) \\ & + \epsilon^2 \frac{\partial}{\partial y} \left(\eta(\theta)\eta'(\theta) \frac{\partial \phi}{\partial x} \right) \\ & + \epsilon^2 \nabla(\eta^2(\theta)\nabla\phi), \end{aligned} \quad (3.4)$$

$$\frac{\partial u}{\partial t} + \frac{1}{\Delta}(30\phi^2 - 60\phi^3 + 30\phi^4) \frac{\partial \phi}{\partial t} = \nabla^2 u. \quad (3.5)$$

Here ϕ is the order parameter or phase field ($\phi = 0$ corresponds to the smectic-B phase, while $\phi = 1$ to the nematic phase) and $u = (T - T_{ns})/\Delta T$ is the dimensionless temperature, where ΔT is the undercooling. The local interface orientation is calculated from the relation $\tan(\theta) = \partial_y \phi / \partial_x \phi$. Lengths have been scaled in some arbitrary reference length ω (see below), whereas time is measured in units of ω^2/D . The dimensionless parameters that characterize the model (besides $\eta(\theta)$) are defined as

$$\begin{aligned} \Delta &= c_p \Delta T / L, \\ \beta &= \frac{\sqrt{2}\omega L^2}{12c_p \sigma(0)T_{ns}} = \frac{\sqrt{2}\omega}{12d_0}, \\ \epsilon &= \delta/\omega, \end{aligned} \quad (3.6)$$

$$\tau(\theta) = \frac{LD}{\sigma(0)T_{ns}} \frac{\eta(\theta)}{\mu(\theta)} = \frac{c_p D}{Ld_0} \frac{\eta(\theta)}{\mu(\theta)}, \quad (3.7)$$

where d_0 is the capillary length, δ the interface thickness (we remind that $\eta(\theta) = \sigma(\theta)/\sigma(0)$).

4. Numerical method and results

The phase-field model equations (3.4) and (3.5) have been solved numerically in a rectangular lattice with scaled dimensions X_L and Y_L in the x and y coordinate directions, respectively. Both equations have been discretized spatially using first-order finite differences on a uniform grid with mesh spacing Δx . We have employed an explicit time-differencing scheme for the equation for the phase-field variable ϕ , so the time step Δt has been adjusted in each case in order to avoid numerical instability. For the heat equation an

explicit scheme would have imposed much stronger restrictions on Δt , therefore it has been solved using the alternating-direction implicit method (ADI), which is unconditionally stable [30]. We have always simulated one quarter of the full experimental system by locating the initial smectic-B seed ($\phi = 0, u = 0$) in the lower left corner. We set $\phi = 1, u = -1$ initially in the rest of the system. Symmetric (reflecting) boundary conditions for ϕ and u have been imposed on the four sides of the system.

We have taken in our simulations $\tau(\theta) = m\eta(\theta)$, with constant m , which implies that the kinetic term remains isotropic (function $\mu(\theta)$ constant, see Eq. (3.7)). $\eta(\theta)$ is taken from Eq. (2.1) for substances I and II. Since $\eta''(\theta)$ is singular in the faceting direction $\theta = 90^\circ$ the question of regularization of the relevant terms in Eq. (3.4) arises. The spatial discretization of the phase field equations provides a natural regularization procedure. If derivatives are performed numerically as they are written in Eq. (3.4), no special care is required to obtain robust results. If the derivatives are developed before numerical discretization, a term with a coefficient proportional to $\delta(\theta - \frac{1}{2}\pi)$ will appear, which will require special attention. The prescription equivalent to the former procedure would be to assign a weight $\delta(0) \sim 1/\Delta x$ whenever the argument of the delta function changes sign.

The parameters β and ϵ (and finally also m , see below) of the model have had to be adjusted after some test running. One can give the following guide lines: It is convenient to choose ω as large as the longest relevant spatial scale, which is due to thermal diffusion. One would normally choose the size of the system somewhat larger than ω , so we took typically $X_L = Y_L$ of the order of 1.5. Then, clearly, β has to be chosen very large (d_0 is a microscopic quantity). ϵ should be chosen for the interface thickness to be smaller than the evolving dendritic structure (smallest radius of curvature of the germ) in order to approximate the sharp-interface limit. The numerical accuracy is satisfactory when Δx is chosen close to ϵ . In some cases we have checked that decreasing Δx did not affect the results substantially. Note that selecting the parameters β and ϵ within these ranges should lead (and indeed lead) to results that are independent of the precise choice.

The parameter values employed for substance I are $\Delta x = 0.005$, $\beta = 350$, $\epsilon = 0.005$, $m = 20$, except in the case of large undercooling, where we have used $\beta = 450$, $\epsilon = 0.003$, $m = 14$. (Note that, as a consequence of the arbitrariness of the length scale ω , the discretized system is invariant under the transformation $\beta \rightarrow z\beta$, $\epsilon \rightarrow \epsilon/z$, $\Delta x \rightarrow \Delta x/z$, keeping the other parameters, including the number of grid points, fixed.) For substance I the time step Δt varied from 10^{-4} to 9×10^{-6} when going from the smallest to the largest undercooling values. The parameter values employed for substance II are $\beta = 350$, $\epsilon = 0.005$, $m = 20$ and $\Delta x = 0.003$ for small undercooling and $\Delta x = 0.005$ for large undercooling. Time step Δt varied from 1.2×10^{-5} to 5×10^{-6} . Numerical simulations for substance II require smaller time steps than those of substance I because of the deeper cusp present in the function $\eta(\theta)$.

Employing the simulation parameters previously mentioned, the four main morphologies of substance I have been computationally reproduced in a square domain of typically 300×300 grid points, except in the case of large Δ , where a 500×500 grid points domain has been used. In order to avoid prohibitively long computation times, we have employed dimensionless undercoolings approximately one order of magnitude larger than those used in the experiments. The quasi-equilibrium shape has been simulated using a dimensionless undercooling $\Delta = 0.05$ and a time step $\Delta t = 10^{-4}$ (Fig. 3(a)). The width-to-length ratio is 1 : 5, which is very similar to the experimental value. Second and third (the butterfly) morphologies (Figs. 3(b) and (c)) of substance I are reproduced using $\Delta = 0.09$ and $\Delta = 0.2$, respectively. Facets tend to vanish and the branch continuously opens up. The beginning of a side branching activity emerging from the lower (rough) side of the main dendrite is observed.

When the undercooling is increased to a value of 0.5 or larger, our simulation is in the equivalent stage to that leading to the dendritic morphology in the experimental description. Here the large value of Δ forced us to use a smaller time step ($\Delta t = 9 \times 10^{-6}$). A fast moving dendrite grows forming a well-defined angle α between its main branches (angle $\frac{1}{2}\alpha$ between the x -axis and the branch seen in Fig. 3(d)). Side branches

appear on both sides of the main branch, tending to orient themselves at an angle $-\frac{1}{2}\alpha$, i.e. parallel to the other main branch. Some tertiary side arm activity has

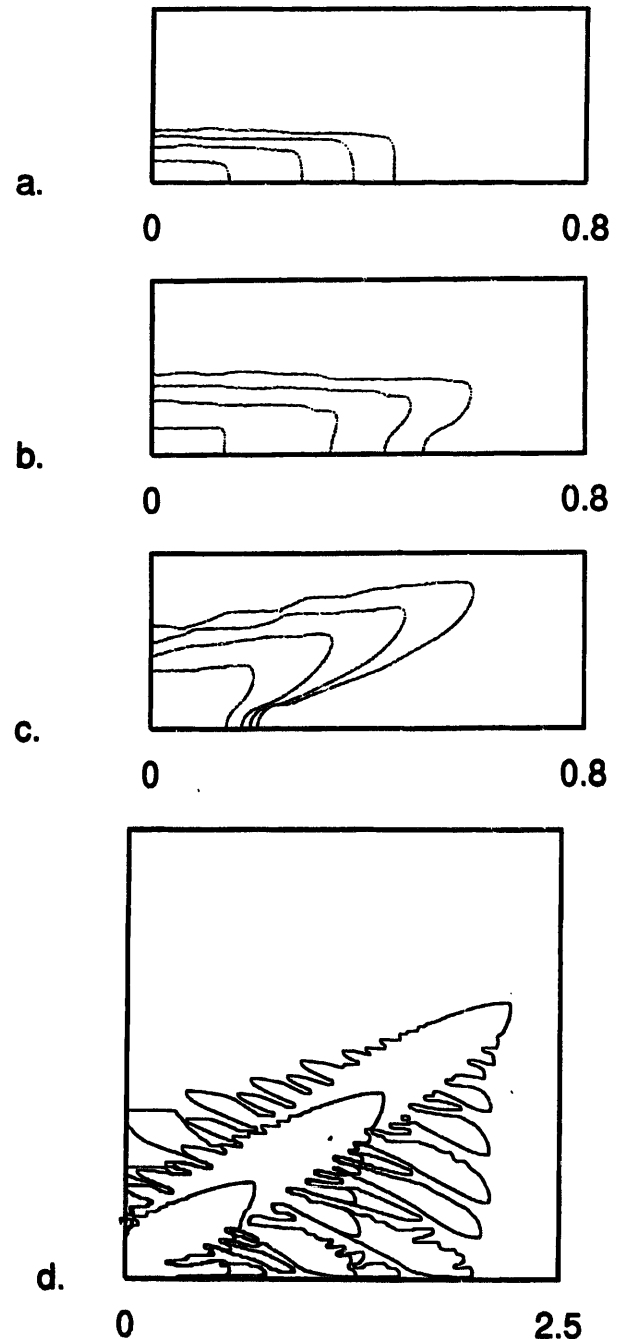


Fig. 3. Substance I. Nematic-smectic-B interface obtained from simulation at subsequent times: (a) $\Delta = 0.05$, $t = 0.14, 0.42, 0.70, 0.98$; (b) $\Delta = 0.09$, $t = 0.08, 0.32, 0.56, 0.80$; (c) $\Delta = 0.2$, $t = 0.06, 0.12, 0.18, 0.24$; (d) $\Delta = 0.7$, $t = 0.033, 0.066, 0.099$; (a), (b) and (c): 300×300 grid points, $\epsilon = \Delta x = 0.005$, $\beta = 350$, $m = 20$, $\Delta t = 10^{-4}$; (d): 500×500 grid points, $\epsilon = 0.003$, $\Delta x = 0.005$, $\beta = 450$, $m = 14$, $\Delta t = 9 \times 10^{-6}$.

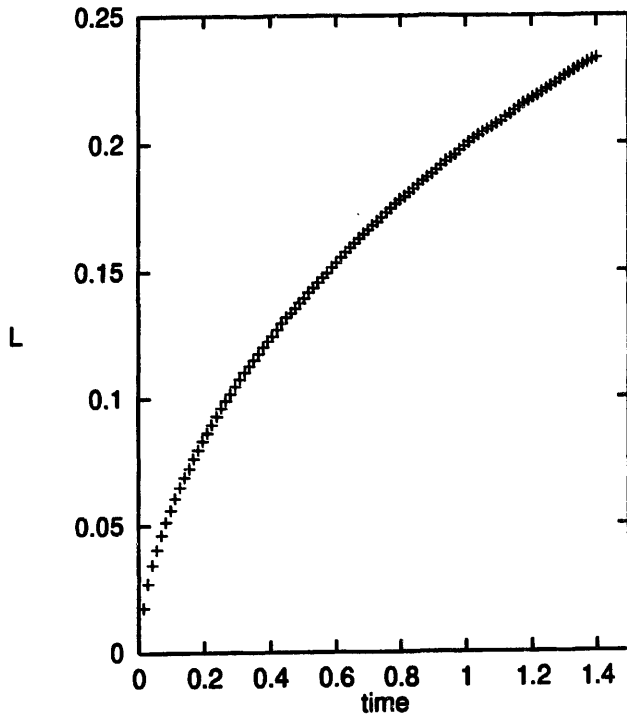


Fig. 4. Substance I. Square root of the area occupied by the smectic-B phase versus time computed from simulation in the quasi-equilibrium regime. Parameters are as in Fig. 3(a).

also been observed, but a large amount of computation time is usually required for such processes. α is noticeably smaller than 90° , which is the angle found for substance I.

In the quasi-equilibrium regime ($\Delta = 0.05$) a spatially averaged growth velocity v has been determined by considering $L = \sqrt{A}$ ($A =$ area of the germ, i.e. area with $\phi = 0$) versus time, see Fig. 4, and setting $v = d\sqrt{A}/dt$. A dependence $v \sim t^{-\gamma}$ is observed, where a value of γ obtained from our simulations was 0.46. For long times the velocity tended to become constant. Then finite-size effects cannot be ruled out.

For substance II we have computationally reproduced the morphologies corresponding to quasi-equilibrium and to large undercooling, where one has dendritic-like growth. The computational domains were 300×300 and 500×500 grid points, respectively. The quasi-equilibrium shape of substance II has been obtained with a dimensionless undercooling $\Delta = 0.075$ and time step $\Delta t = 1.2 \times 10^{-5}$ (Fig. 5(a)). This shows a more elongated shape than substance I, in agreement with the experiment.

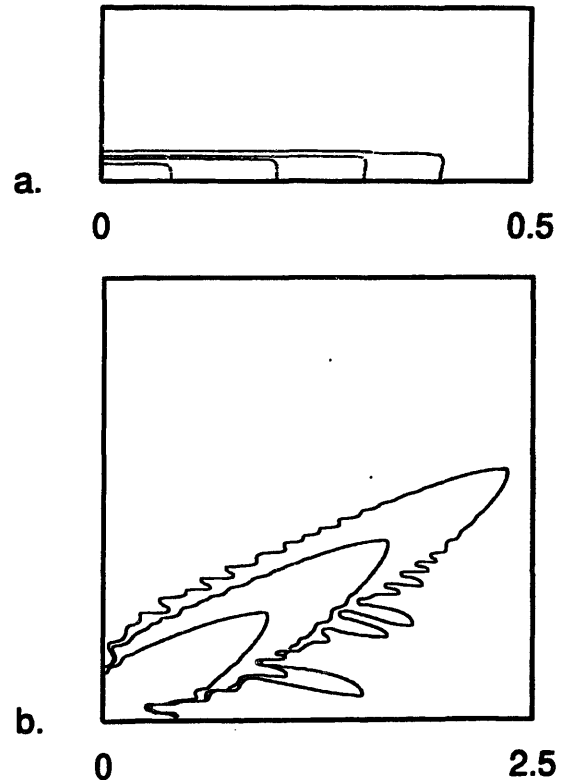


Fig. 5. Substance II. Nematic-smectic-B interface obtained from simulation at subsequent times (a) $\Delta = 0.075$, $t = 0.03, 0.09, 0.15, 0.21$; (b) $\Delta = 0.5$, $t = 0.104, 0.182, 0.260$; (a): 300×300 grid points, $\epsilon = 0.005$, $\Delta x = 0.003$, $\beta = 350$, $m = 20$, $\Delta t = 1.2 \times 10^{-5}$; (b): 500×500 grid points, $\epsilon = \Delta x = 0.005$, $\beta = 350$, $m = 20$, $\Delta t = 5 \times 10^{-6}$.

In order to reproduce the dendritic shape at $\Delta = 0.5$ we were forced to decrease the time step to $\Delta t = 5 \times 10^{-6}$. The morphology obtained (Fig. 5(b)) corresponds to one observed experimentally, see Fig. 2. (We remind that the experiments in substance II exhibit some variability.) Again there is a single angle α that characterizes the direction of the main side branches.

5. Concluding remarks

In this work we were able to reproduce the basic growth morphologies of smectic-B germs into the supercooled nematic phase of two liquid crystals, by means of phase-field simulations. There are two main conclusions to be drawn. The first, on a methodological level, is that in the phase-field approach one can handle strongly anisotropic interfaces and particularly

faceting in a rather simple way, rendering such situations computationally feasible. Without refinements, and in particular with our resources (mainly a medium-powered Risc workstation), one is at present restricted to fairly small systems, which is a result of the very different space scales entering the problem in the phase-field approach. This disparity increases with decreasing undercooling, which is illustrated e.g. by the behaviour of the Péclet number $p \approx \Delta^2/\pi$, which gives the ratio between the tip radius ρ of an Ivantsov needle crystal moving at velocity v and the thermal diffusion length $l = 2D/v$, at low undercooling Δ (see e.g. [39]). Therefore, one has to resort to undercoolings larger than those employed in the experiments in order to see qualitatively the same effects. As a consequence, one cannot at this point make a quantitative comparison, which would also require a better knowledge of the relevant material parameters, in particular the kinetic coefficient (including its anisotropy). In order to get to smaller undercooling one would have to use more sophisticated numerical techniques where the long-range temperature field outside the germ is treated separately.

The second conclusion, which we can draw (in spite of the present limitations of the method) is that the anisotropy provided by the surface tension is the most important factor in determining the morphologies in the complex growth processes observed in the experiments. This is actually rather surprising in view of the sophisticated ordering process taking place in the nematic smectic-B transition. However, details of the shapes at larger undercooling depend on the kinetic term, whose magnitude m was chosen such that its influence became noticeable at the velocities involved when the fourth morphology appeared. The isotropic kinetic term used here has the effect of opening up the branches, compared to a situation where τ is chosen independent of angle. Preliminary tests with the parameters of Fig. 3(d), but with isotropic τ , display a much smaller opening angle and no side branching, so the morphology reacts sensitively to the angular dependence of the kinetic term. A direct measurement of the kinetic coefficient would be desirable, but it would involve measuring the growth velocity at much larger undercooling than was reachable experimentally. The

kinetic coefficient, including its anisotropy, has been measured for impurity controlled growth of a hexagonal columnar mesophase [40].

The main remaining discrepancy is that for substance I the apparent fourfold symmetry (α close to 90°), which is found in the experiments in the fourth morphology, see Fig. 1(d), is not reproduced very convincingly in the simulations. In the experiments the dendrite tips become manifestly parabolic, which is also not seen very clearly in the simulations (see Fig. 3(d)). There is hope that tailoring the anisotropy of the kinetic term appropriately will improve the situation. We will check this in future work.

Another concern about the way kinetic effects are incorporated in the model relates to the fact that, when facets are present, the dependence of the kinetic term in the Gibbs–Thomson relation may not be strictly linear in the normal velocity. Other forms have been discussed in the literature (see Chapter 2; [2,17]). In contrast to the anisotropy of the kinetic effects, a non-linear dependence on the velocity cannot be handled by the phase-field model in its present form, and more drastic modifications should be introduced to properly incorporate such effects. However, in view of the qualitative agreement with the experiments, these effects do not seem to affect the basic features.

There may also be other reasons for the discrepancy, which could lend support to another interesting, and as yet not understood observation. It was found in previous experiments [28] that the rapidly grown smectic-B phase of substance I, i.e. that grown via the fourth morphology, had somewhat different properties than the ones grown slower. Upon increase of the temperature the melting temperature of the rapidly grown phase was found to be noticeably decreased and moreover the shape of the nematic germs inside the smectic-B (“negative germs”) was totally different from that of the positive germs. They had an oval shape (no faceting) with an anisotropy opposite to that of the positive germs. Thus the smectic-B phase of substance I might be of a different nature (presumably less ordered) when grown rapidly than when grown slower. Possibly this is of relevance for the growth of dendrites in the fourth morphology of substance I. However, the rapid growth cannot be described by simply

replacing the cusped function $\eta_1(\theta)$ of Eq. (2.1) by one appropriate for the oval negative germs, because that function does not exhibit the appropriate symmetry either. In substance II, which does not exhibit the symmetric dendrites, the negative germs were mostly found to have also an oval shape with some exceptions, when a partial faceting of the interface could be detected. More detailed experimental investigations are in progress.

In our description we have only included the effect of heat diffusion neglecting the influence of impurity diffusion. We believe that this is justified. First of all, the materials used are known to be chemically very pure and stable, at least in the room-temperature crystalline phase. Moreover in the normal course of the experiments no considerable coexistence range of the two liquid crystalline phases could be observed. This changed when substance I was kept in a liquid crystalline state for a time exceeding about a normal working day. Then, on a slow time scale, the behaviour changed: The nematic smectic-B transition temperature decreased, the equilibrium shapes of smectic-B germs changed in the direction of less anisotropy (the faceted side became shorter), a range of coexistence developed (up to about 2°C), and the growth dynamics slowed down drastically (details will be presented elsewhere). The effects could be reversed, at least partially, by crystallizing the substance and going repeatedly through the crystal nematic phase transition. This then indicates that in the liquid crystalline state the substance experiences a (reversible) chemical transformation, most likely an isomerization. Presumably the isomer is expelled from the smectic phase. Since these effects are quite well under control we are particularly confident that impurities play a minor role in the experiments discussed here.

In future work we hope to obtain a better analytic understanding of the morphologies observed experimentally and numerically, and to enter into a more quantitative stage. This may elucidate to what extent three-dimensional effects, wetting, etc. affect the experimental results. A particularly challenging selection problem is posed by the opening angle α of the branches of the dendrite, which appears to characterize the morphology rather completely under rapid-growth

conditions. There is some evidence from experiments as well as simulations that this angle is not determined by initial conditions, but is an intrinsic dynamical property of the growth process. Eventually it may also become important to consider the fact that in the experimental system heat is not removed through the distant lateral boundaries, but rather through the upper and lower glass plates of the layer. This provides a spatial cut-off for the otherwise long-ranged thermal diffusion field and leads to the existence of (unstable) planar front solutions moving with constant velocity at any undercooling.

Acknowledgements

We acknowledge European Commission (TMR Programme, project ERB-4061-PL-95-1377) for support. RGC, LRP, JC and AHM thank the Dirección General de Investigación Científica y Técnica (Spain) (Projects PB93-0769-C02-02 and PBR93-0054-C02-01) for support. JC and AHM acknowledge NATO (Collaborative Research Grant No. 931018) for support. We also acknowledge the Centre de Supercomputació de Catalunya (CESCA) for computing support. AB and LK are indebted to the University of Barcelona for its kind hospitality and assistance and thank the Volkswagen-Stiftung for support. AB acknowledges support by OTKA T014957. LK is grateful for support through an Alexander von Humboldt-J.C. Mutis Award for the Scientific Cooperation between Spain and Germany.

References

- [1] P. Pelcé, ed., *Dynamics of Curved Fronts, Perspectives in Physics* (Academic Press, New York, 1988).
- [2] C. Godrèche, ed., *Solids far from Equilibrium* (Cambridge University Press, Cambridge, 1992).
- [3] D.T.J. Hurle, ed., *Handbook of Crystal Growth*, Vol. 1B (North-Holland, Amsterdam, 1993).
- [4] P.E. Cladis and P. Palfy-Muhoray, eds., *Spatio-Temporal Patterns*, Santa Fe Institute Studies in the Science of Complexity, Vol. XXI (Addison-Wesley, Reading, MA, 1994).
- [5] P.P. Trigueros, J. Claret, F. Mas and F. Sagués, *J. Electroanal. Chem.* 312 (1991) 219.

- [6] E. Ben-Jacob and P. Garik, *Nature* 343 (1990) 523.
- [7] D. Kessler, J. Koplik and H. Levine, *Adv. in Phys.* 37 (1988) 255.
- [8] E.A. Brener and V.I. Melnikov, *Adv. in Phys.* 40 (1991) 53.
- [9] J. Maurer, P. Buisson, B. Perrin and P. Tabeling, *Europhys. Lett.* 8 (1989) 67.
- [10] M. Ben Amar and Y. Pomeau, *Europhys. Lett.* 6 (1988) 609.
- [11] J.E. Taylor, *Act. Metall. Mater.* 40 (1992) 1475.
- [12] M. Adda Bedia and V. Hakim, *J. de Phys. (France)* 4 (1994) 383.
- [13] M. Adda Bedia and M. Ben Amar, *Faceting in the Free Dendritic Growth*, in: Thèse de Doctorat, author M. Adda Bedia, Paris 1994, *Phys. Rev. E* 51 (1995) 1268.
- [14] R. Bowley, B. Caroli, C. Caroli, F. Graner, P. Nozières and B. Roulet, *J. de Phys. (France)* 50 (1989) 1377.
- [15] B. Caroli, C. Caroli and B. Roulet, *J. de Phys. (France)* 50 (1989) 3075.
- [16] M. Adda Bedia and M. Ben Amar, *Phys. Rev. A* 10 (1991) 5702.
- [17] P. Oswald and F. Melo, *J. Phys. II (France)* 2 (1992) 1345.
- [18] J. Bechoefer, P. Oswald, A. Libchaber and C. Germain, *Phys. Rev. A* 37 (1988) 1691.
- [19] F. Melo and P. Oswald, *Phys. Rev. Lett* 64 (1990) 1381.
- [20] F. Melo and P. Oswald, *J. Phys. II (France)* 2 (1991) 353.
- [21] D.K. Shangguan and J.D. Hunt, *Metall. Trans. A* 22 A (1991) 941.
- [22] L.M. Fabietti and R. Trivedi, *Metall. Trans. A* 22 A (1991) 1249.
- [23] N. Dey and J.A. Sekhar, *Act. Metall. Mater.* 41 (1993) 409.
- [24] G.W. Gray and J.W.G. Goodby, *Smectic Liquid crystals*. (Leonard Hill, Glasgow, 1984) Chapter 10.
- [25] G. Vertogen and W.H. de Jeu, *Thermotropic Liquid Crystals, Fundamentals* (Springer, Berlin, 1988) Chapter 3.
- [26] Á. Buka and N. Éber, *Europhys. Lett.* 21 (1993) 477.
- [27] Á. Buka, T. Tóth Katona and L. Kramer, *Phys. Rev. E* 51 (1995) 571.
- [28] Á. Buka, T. Tóth Katona and L. Kramer, *Phys. Rev. E.* 49 (1994) 5271.
- [29] R. Kobayashi, *Physica D* 63 (1993) 410.
- [30] A.A. Wheeler, B.T. Murray and R.J. Schaefer, *Physica D* 66 (1993) 243.
- [31] G.B. McFadden, A.A. Wheeler, R.J. Braun, S.R. Coriell and R.F. Sekerka, *Phys. Rev. E* 48 (1993) 2016.
- [32] S.-L. Wang, R.F. Sekerka, A.A. Wheeler, B.T. Murray, S.R. Coriell, R.J. Braun and G.B. McFadden, *Physica D* 69 (1993) 189.
- [33] R.J. Braun, G.B. McFadden and S.R. Coriell, *Phys. Rev. E* 49 (1994) 4336.
- [34] R. Kupferman, O. Shochet and E. Ben-Jacob, *Phys. Rev. E* 50 (1994) 1005.
- [35] A. Bosch, H. Muller-Krumbhaar and O. Shochet, *Z. Phys. B* 97 (1995) 367.
- [36] F. Liu and M. Goldenfeld, *Phys. Rev. A* 42 (1990) 5052.
- [37] T. Tóth Katona, T. Börzsönyi, Z. Varadi, J. Szabon, A. Buka, R. González-Cinca, L. Ramírez-Piscina, J. Casademunt and A. Hernández-Machado, to be published.
- [38] G. Caginalp, *Arch. Rational Mech. Anal.* 92 (1986) 205 *Phys. Rev. A* 38 (1989) 5887.
- [39] J.S. Langer, in: *Chance and Matter*, eds. J. Souletie, J. Vannimenus and R. Stora, Les Houches, Session XLVI (North-Holland, Amsterdam, 1987) Chapter 10.
- [40] J.C. Geminard, P. Oswald, D. Temkin and J. Malthete, *Europhys. Lett.* 22 (1) (1993) 69.